**Combined Effect of Citrate and Fluoride Ions on Hydroxyapatite Nanoparticles**

# Combined effect of citrate and fluoride ions on hydroxyapatite nanoparticles

Lorenzo Degli Esposti[a,*], Alessio Adamiano[a], Anna Tampieri[a], Gloria Belen Ramirez-Rodriguez[b], Dritan Siliqi[c], Cinzia Giannini[c], Pavlo Ivanchenko[d], Gianmario Martra[d], Feng-Huei Lin[e,f], José Manuel Delgado-López[b], Michele Iafisco[a,*]

[a]Institute of Science and Technology for Ceramics (ISTEC), National Research Council (CNR), Via Granarolo 64, 48018 Faenza (Italy)

[b]Department of Inorganic Chemistry, University of Granada, Av. Fuente Nueva, s/n, 18071, Granada (Spain)

[c]Institute of Crystallography (IC), National Research Council (CNR), Via Amendola 122/O, 70126 Bari (Italy)

[d]Department of Chemistry and Interdepartmental Centre "Nanostructured Interfaces and Surfaces-NIS", University of Torino, Via P. Giuria 7, 10125, Torino (Italy)

[e]Department of Biomedical Engineering, National Taiwan University, 10617 Taipei (Taiwan)

[f]Institute of Biomedical Engineering and Nanomedicine, National Health Research Institutes, Keyan Road 35, 35053 Miaoli (Taiwan)

Authors for correspondence:

Dr. Michele Iafisco, Ph. D.
Institute of Science and Technology for Ceramics (ISTEC) National Research Council (CNR),
Via Granarolo 64, 48018 Faenza (RA), Italy.
E-mail: michele.iafisco@istec.cnr.it

Lorenzo Degli Esposti, M. Sc.
Institute of Science and Technology for Ceramics (ISTEC) National Research Council (CNR),
Via Granarolo 64, 48018 Faenza (RA), Italy.
E-mail: lorenzo.degliesposti@istec.cnr.it

**FT-IR spectra of citrate-HA.** The IR-ATR spectra of the citrate-HA samples are reported in Figure S1B. All samples displayed a main broad band at 1030 $cm^{-1}$ with shoulders at 1046 and 1075 $cm^{-1}$ due to the triply degenerated anti-symmetric stretching mode of the apatitic $PO_4$ groups ($\nu_3PO_4$). Other features emerge at 961 $cm^{-1}$ (symmetric stretching mode of the apatitic $PO_4$ groups, $\nu_1PO_4$) and at 603, 576 (as a shoulder) and 565 $cm^{-1}$ (triply degenerated bending mode of the same groups, $\nu_4PO_4$). Apatitic hydroxyl groups are evinced by a band at 631 $cm^{-1}$ that is due to $OH^-$ librational modes [1]. The presence of traces amounts of carbonate ions is revealed by the presence of a very weak B-type carbonate substitution ($CO_3$ occupying $PO_4$ sites) band at 873 $cm^{-1}$ [2].

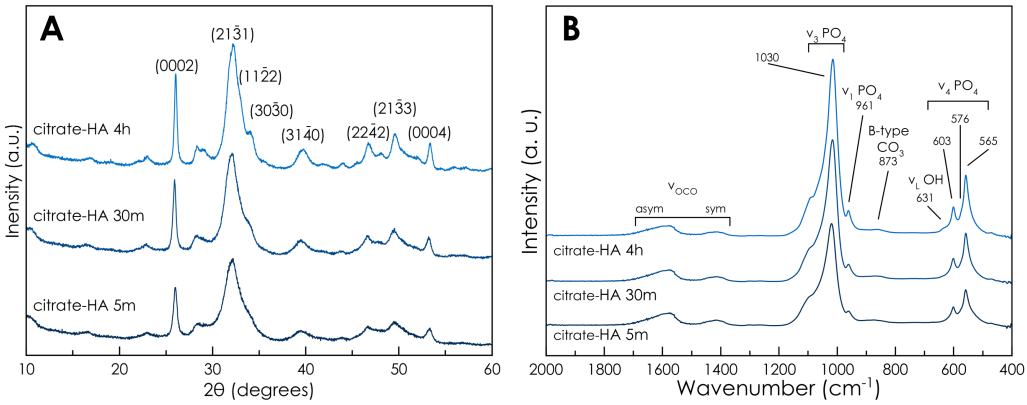


**Figure S1.** (A) PXRD diffractograms of citrate-HA 5m, citrate-HA 30m, and citrate-HA 4h. (B) FT-IR spectra of citrate-HA 5m, citrate-HA 30m, and citrate-HA 4h.

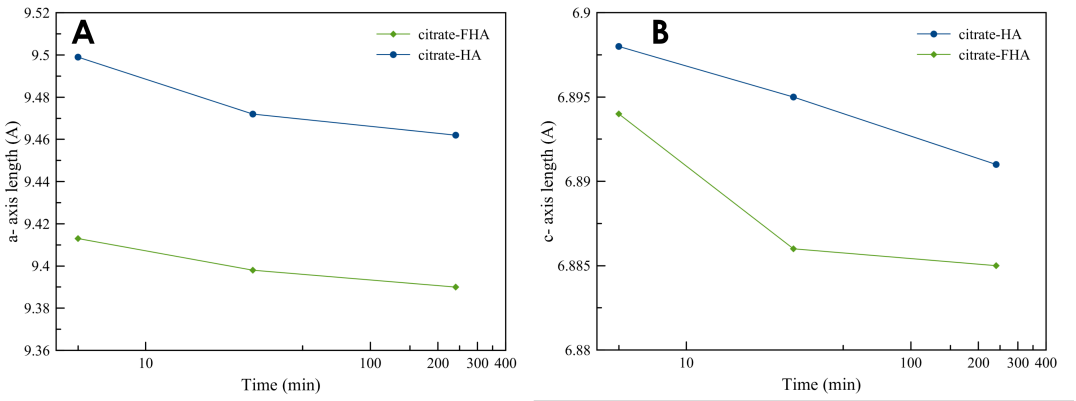


**Figure S2.** Plot as a function of the maturation time of (A) *a* cell axis, (B) *c* cell axis of citrate-FHA and citrate-HA.

**Table S1.** Cell parameters and crystal domain of citrate-HA samples.

| Sample | *a-b* cell axes (Å) | *c* cell axis (Å) | $D_{(0002)}$ (nm) | $D_{(31-40)}$ (nm) | $D_{(0002)}$/ $D_{(31-40)}$ |
|---|---|---|---|---|---|
| Citrate-HA 5m | 9,499 | 6,898 | 21,6±0,5 | 5.5±0,4 | 3,9 |
| Citrate-HA 30m | 9,472 | 6,895 | 28,6±0,5 | 6,3±0,7 | 4,3 |
| Citrate-HA 4h | 9,462 | 6,891 | 42,9±0,5 | 7.3±0,6 | 5,9 |

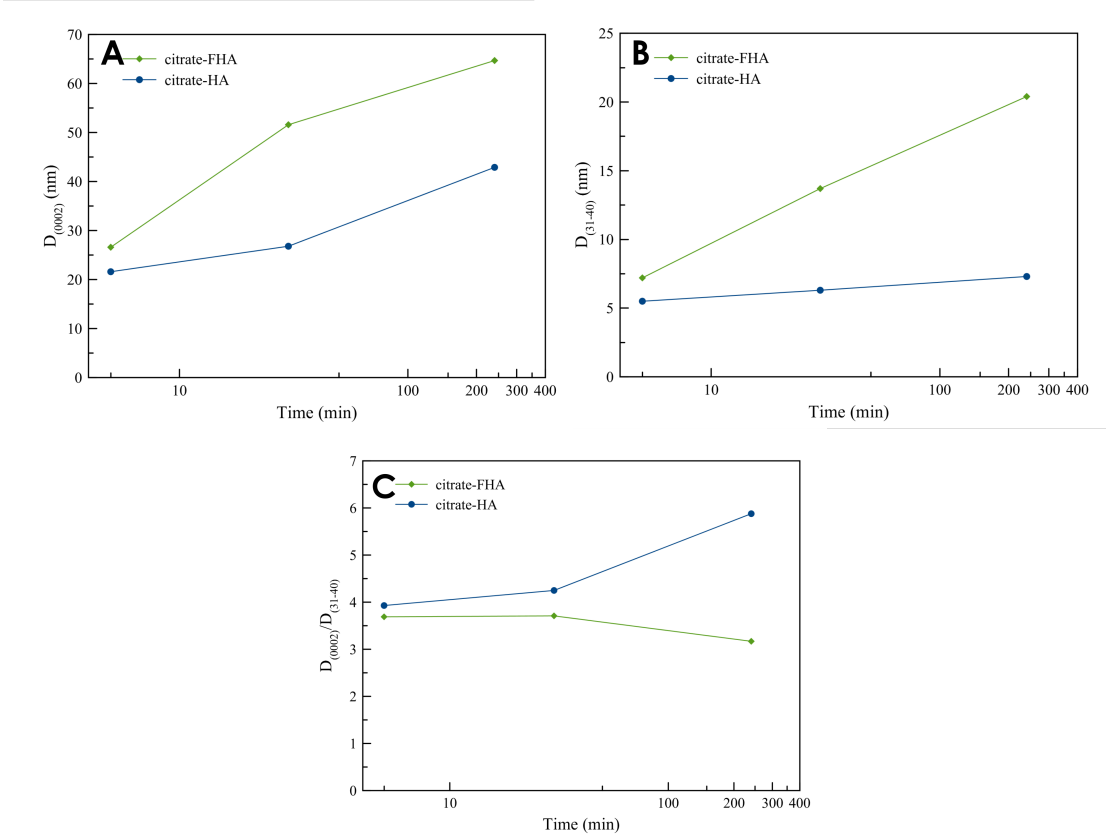


**Figure S3.** Plot as a function of the maturation time of (A) $D_{(0002)}$ crystal domain, (B) $D_{(31-40)}$ crystal domain and (C) $D_{(0002)}/D_{(31-40)}$ ratio of citrate-FHA and citrate-HA.

**Table S2.** Chemical composition of citrate-HA samples.

| Sample | Ca/P[a] (mol) | F[b] (% wt) | Citrate[c] (% wt) | Carbonate[c] (% wt) | ζ-Potential (mV) |
|---|---|---|---|---|---|
| Citrate-HA 5m | 1,54±0,02 | - | 4,8±0,3 | 1,4±0,2 | -13.1 ± 0.4 |
| Citrate-HA 30m | 1,54±0,02 | - | 3,2±0,3 | 0,8±0,1 | -12.4 ± 0.4 |
| Citrate-HA 4h | 1,53±0,01 | - | 2,6±0,2 | 1,2±0,1 | -9.3 ± 0.4 |

[a]Quantified by ICP-OES; [b]Quantified by fluoride ion electrode; [c]Quantified by TGA.

**Thermogravimetric analysis.** Thermogravimetric curves and their first derivatives of all the samples mainly shows four weight losses (Figure S4): (i) from room temperature to 200°C due to the adsorbed water, (ii) from 200°C to 400°C related to structural water, (iii) from 400 to 600°C due to the citrate, and (iv) from 600 to 1000°C corresponding to the carbonate ions [3].

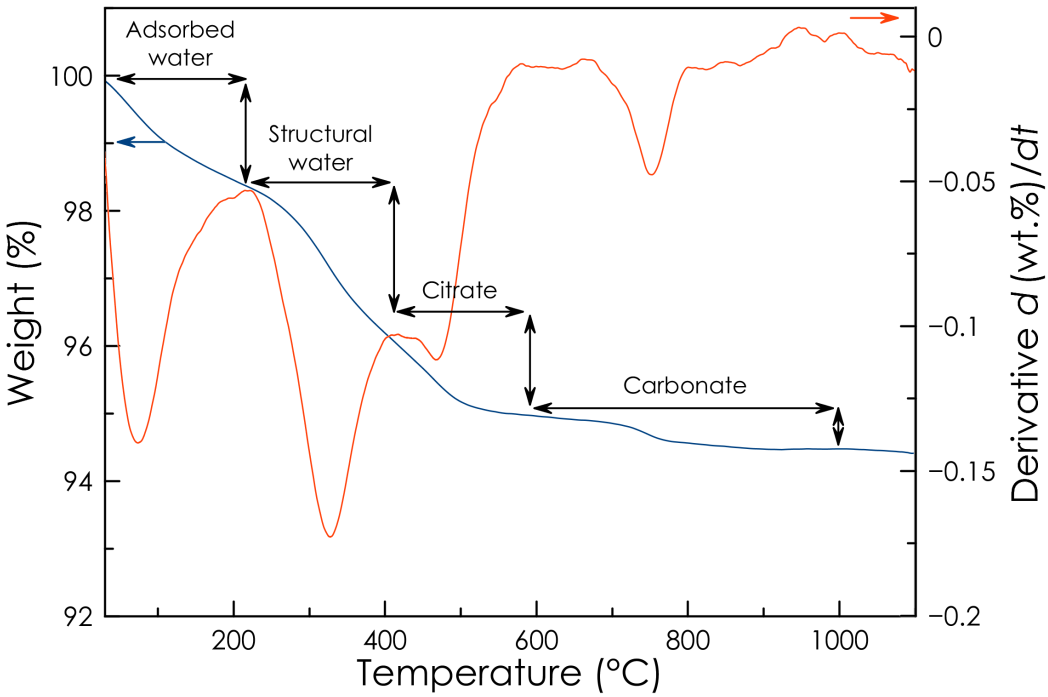


**Figure S4.** TGA and DTG curve of citrate-FHA 4h. The TGA curves of the other samples have the same profile.

**Raman spectroscopy.** Figure S5A-B shows the Raman spectra of the samples. The most intense peak appears at 960 $cm^{-1}$, which corresponds to $\nu_1PO_4$ mode. Other features from apatitic $PO_4$ group emerge at 1042 $cm^{-1}$ ($\nu_3PO_4$), 586 ($\nu_4PO_4$) and 428 $cm^{-1}$ ($\nu_2PO_4$). In the spectrum of both citrate-FHA and citrate-HA nanoparticles, very weak B-type carbonate bands appeared at 1070 $cm^{-1}$ ($\nu_1CO_3$) and at 1430 $cm^{-1}$ ($\nu_2CO_3$), confirming the data of IR-ATR spectra and chemical analysis [2]. Moreover, the Raman spectrum of citrate-HA samples exhibit an intense peak at 3570 $cm^{-1}$ (Figure S5C-D) associated to the apatitic νOH mode. The intensity of this peak increases with maturation time. On the contrary, this band is not present in the spectrum collected for the citrate-FHA nanoparticles, further confirming that $OH^-$ ions were completely replaced by fluoride ions. The bands at 2930 and 845 $cm^{-1}$ are related to the $\nu CH_2$ and the δOCO modes of citrate [4], respectively, and their relative intensity decreases with maturation time as observed in the IR-ATR spectra.

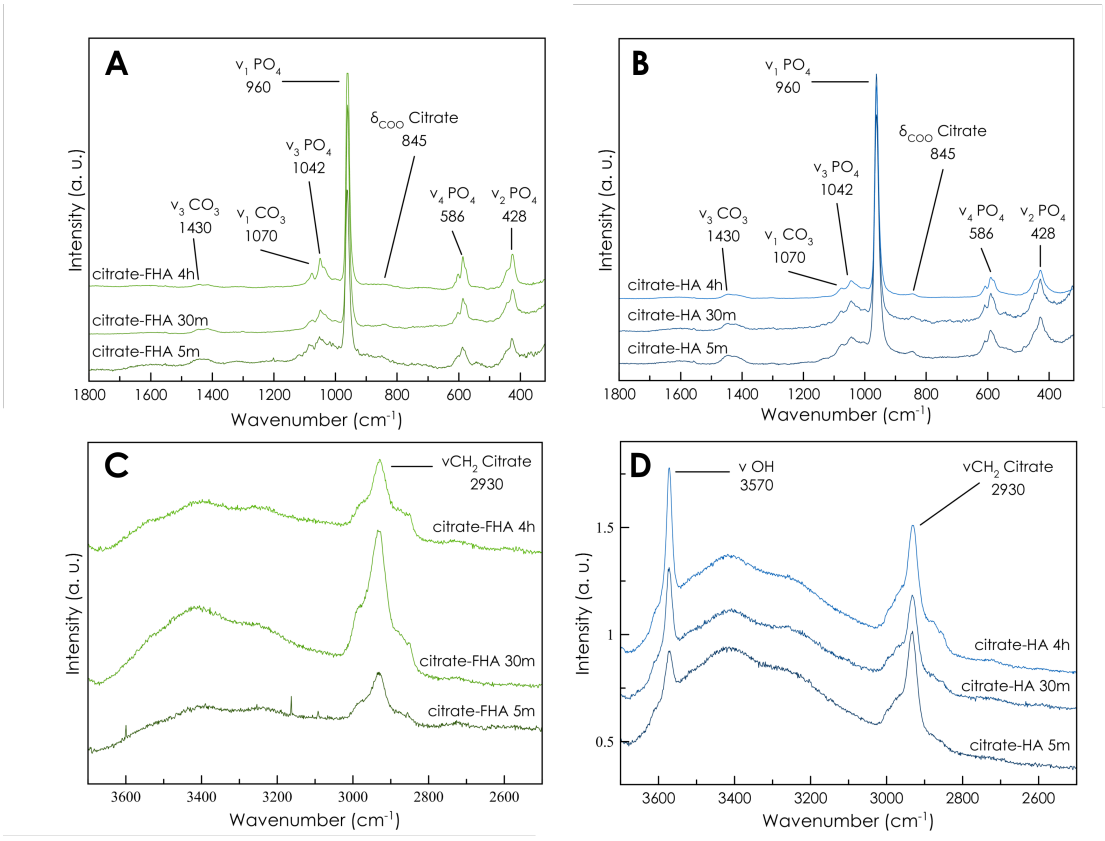


**Figure S5.** Raman spectra of (A) of citrate-FHA 5m, citrate-FHA 30m, citrate-FHA 4h and (B) citrate-HA 5m, citrate-HA 30m, and citrate-HA 4h. (C) and (D) show an enlarged view of the OH and CH stretching modes spectral region for citrate-FHA and citrate-HA, respectively.

**FT-IR spectroscopy in controlled atmosphere mode (Figure S6).** The $\nu_{asym}COO$ mode of citrates falling in 1750-1500 $cm^{-1}$ range overlaps with $\delta H_2O$ mode of adsorbed water (centered at ca. 1645 $cm^{-1}$). Thus, the detailed analysis of citrate profile requires the complete removal of the adsorbed water. To this aim, the sample in contact with $H_2O$ at 20 mbar (curve a) was outgassed at b.t. for 60 min (curve b). Further, surface-accessible water along with OH species was exchanged with $D_2O$ ($\delta$ $D_2O$ is located at 1200 $cm^{-1}$) by 10 cycles of contacting the sample with 20 mbar of $D_2O$ for 5 min followed by 5 min outgassing with subsequent 60 min outgassing at b.t. (curve c). The resulting profile is 'cleaned' from the contribution of water vibrations in the 1750-1500 $cm^{-1}$ range.

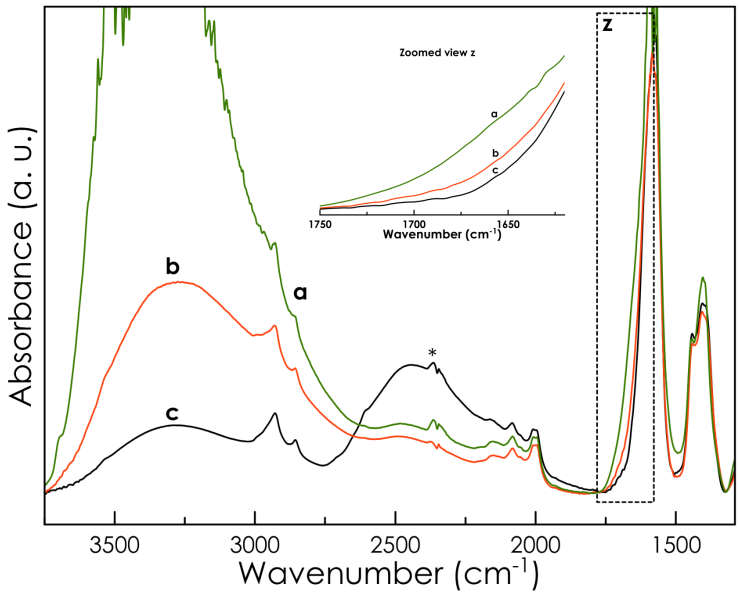


**Figure S6.** FT-IR spectra of citrate-FHA 4h. Curve (a) in contact with $H_2O$ vapor at 20 mbar; curve (b) after 60 min outgassing at b.t.; curve (c) after exchange with $D_2O$ and subsequent 60 min outgassing at b.t. Inset: zoomed view of 1750-1620 $cm^{-1}$ range. *small feature due to non-compensated atmospheric $CO_2$.

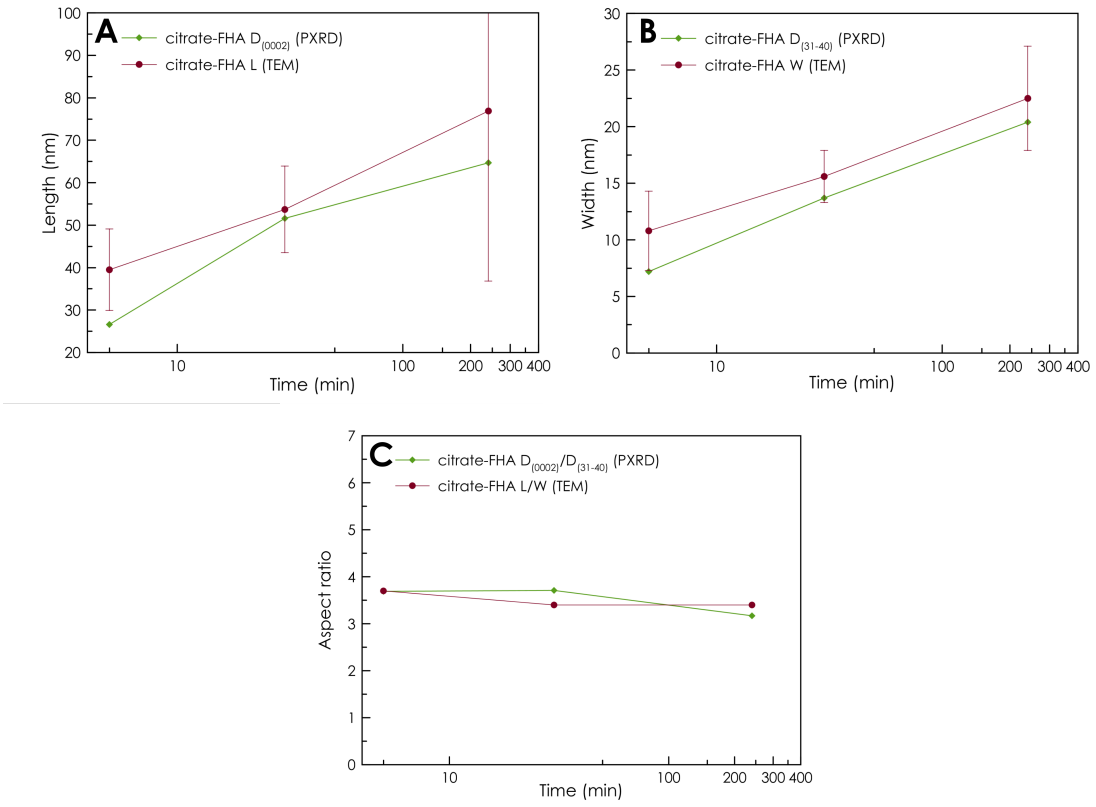


**Figure S7.** Plot as a function of the maturation time of (A) length, (B) width, and (C) aspect ratio of citrate-FHA nanoparticles evaluated by TEM. A comparison with the respective crystal domains calculated by PXRD patterns is reported in each panel.

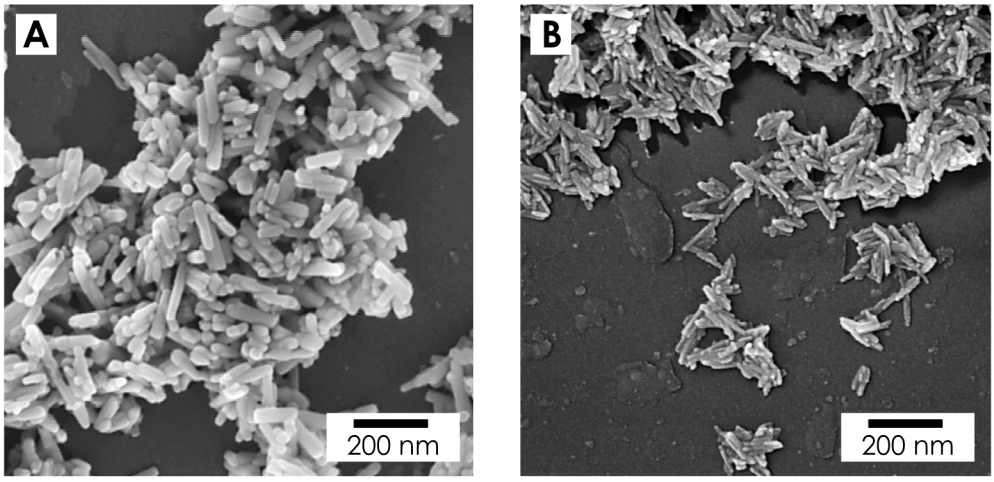


**Figure S8.** FEG-SEM micrographs of (A) citrate-FHA 4h, and (B) citrate-HA 4h.

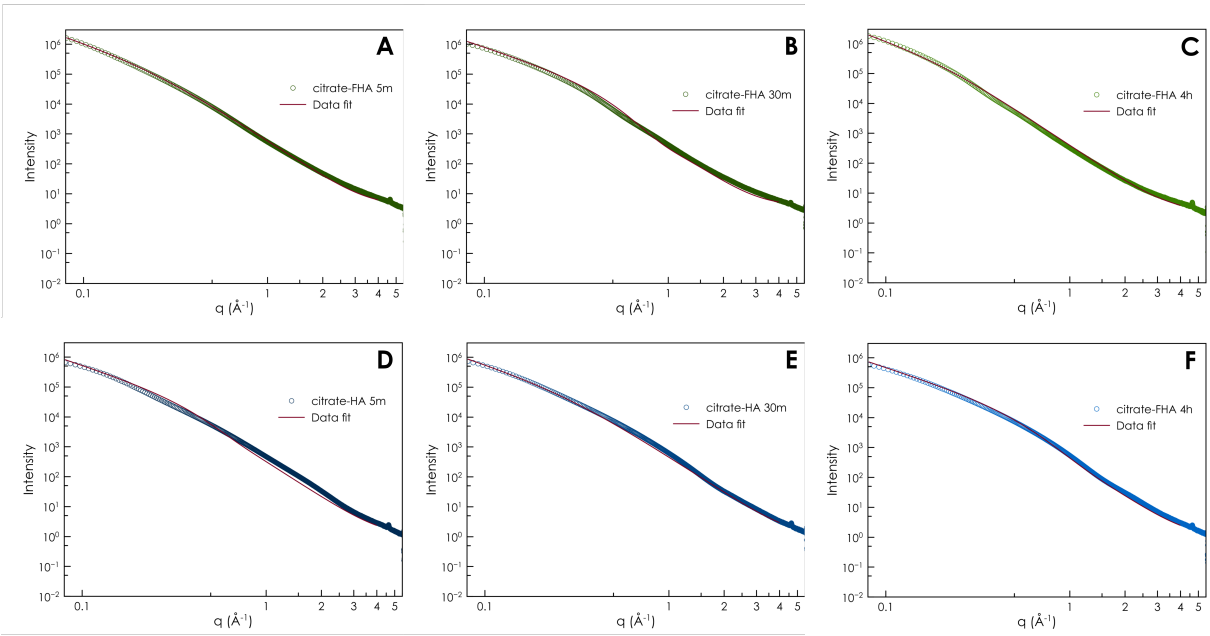


**Figure S9.** SAXS curves and data fitting with lamellar model for (A) of citrate-FHA 5m, (B) citrate-FHA 30m, (C) citrate-FHA 4h, (D) of citrate-HA 5m, (E) citrate-HA 30m, and (F) citrate-HA 4h.

**Table S3.** Mean thickness and polydispersity of citrate-HA samples extracted as lamellar model fitting SAXS data.

| Sample | Thickness (nm) | Polydispersity |
|---|---|---|
| Citrate-HA 5m | 6,8 | 0,47 |
| Citrate-HA 30m | 7,1 | 0,70 |
| Citrate-HA 4h | 5,5 | 0,30 |

## References


1. Koutsopoulos, S., *Synthesis and characterization of hydroxyapatite crystals: a review study on the analytical methods.* Journal of Biomedical Materials Research: An Official Journal of The Society for Biomaterials, The Japanese Society for Biomaterials, and The Australian Society for Biomaterials and the Korean Society for Biomaterials, 2002. **62**(4): p. 600-612.
2. Antonakos, A., E. Liarokapis, and T. Leventouri, *Micro-Raman and FTIR studies of synthetic and natural apatites.* Biomaterials, 2007. **28**(19): p. 3043-3054.
3. Tonsuaadu, K., et al., *A review on the thermal stability of calcium apatites.* Journal of Thermal Analysis and Calorimetry, 2011. **110**(2): p. 647-659.
4. Socrates, G., *Infrared and Raman characteristic group frequencies: tables and charts*. 2004: John Wiley & Sons.